ELSEVIER

Thin Solid Films 381 (2001) 73–83

thin solid films

www.elsevier.com/locate/tsf

Comparison of growth of hydrocarbon thin films by molecular-beam and cluster-beam deposition: atomistic simulations

Thomas A. Plaisted[a], Boris Ni[a], John D. Zahrt[b], Susan B. Sinnott[a,*]

[a] *Department of Chemical and Materials Engineering, University of Kentucky, Lexington, KY 40506-0046, USA*
[b] *Eastern Kentucky University, Richmond, KY 40475, USA*

Received 26 September 1999; received in revised form 19 May 2000; accepted 23 August 2000

Abstract

Molecular dynamics simulations have been performed to study the difference in the growth of polyethylene thin films via neutral ethylene molecular-beam and cluster-beam depositions. The collisions occurred at incident energies of 25 and 50 eV/molecule on a hydrogen-terminated diamond (111) surface. A many-body empirical bond order potential for hydrocarbons was used to model the interatomic interactions in the system that allowed for bonds to be broken and formed over the course of the simulations. In contrast to the expectations that the cluster beam would provide significantly enhanced thin-film nucleation, the results indicate few differences in thin-film adhesion that occurs as a result of the deposition. The role of substrate temperature on thin-film nucleation is also investigated and found to be negligible over a 1200° range. Finally, structural relaxation of thin-film fragments is investigated through energy minimization with AM1. The structures of the fragments are found to change slightly from the relaxed structures predicted in the molecular dynamics simulations.

Keywords: Molecular dynamics; Polyethylene; Thin films

1. Introduction

The bombardment of surfaces with atoms or molecules has been used extensively over the years in such common processes as surface cleaning, chemical vapor deposition, and ion implantation [1]. More recently, interest has also focused on the use of cluster beams to deposit thin films [2]. Clusters are usually small enough to exhibit properties that differ substantially from those of comparable bulk materials [3,4]. When impacted on surfaces they deposit a concentrated amount of energy and material in a very localized region of the surface [5–15]. This can lead to an increased number of chemical reactions between the cluster and surface and the eventual formation of films that in some cases differ considerably from the films that result from single atom or molecule deposition [16]. Experimental work in this area has examined the deposition of metal clusters on metal and carbon substrates [17–21], noble gas [22,23] and silane [24] clusters on ceramic substrates, and phosphide [25] and hydrocarbon [26–28] clusters on glass substrates. In some cases [29,30], strongly adhering organic thin films have been formed through cluster-beam deposition on glass and mica substrates. In these cases, the clusters were estimated to contain either approximately 10 molecules

* Corresponding author. Current address: The University of Florida, Department of Materials Science and Engineering, 100 Rhines Hall, Gainesville, Florida 32611-6400. Tel.: +1-352-846-3778; fax: +1-352-846-3355.
E-mail address: sinnott@engr.uky.edu (S.B. Sinnott).

0040-6090/01/$ - see front matter
PII: S0040-6090(00)01552-2

or large polymeric chains each and were accelerated at incident energies of 250–500 eV/cluster, or 25–50 eV/molecule or chain. At lower thermal velocities amorphous films formed whereas at higher velocities crystalline films resulted [29].

Substrate temperature has also been examined to determine its influence on film formation from cluster–surface interactions. Simulations of the rearrangement behavior of high-temperature clusters on a range of lower temperature substrates predicted that substrate temperature has little effect on film rearrangement [31]. When amorphous carbon films were deposited via plasma beams, however, a transition temperature was found where the sp^2/sp^3 ratio in the film varied because of changes in substrate temperature [32–34]. In another study, increasing substrate temperature was shown to increase the number of microcrystallites in films formed by magnetron sputtering [35].

Cluster-beam deposition of organic material is thought to result in thin-film formation through rapid chemical reactions that occur at the impact site between the cluster and surface. Since these reactions occur on the order of picoseconds (ps), molecular dynamics simulations are well suited to model the mechanisms of thin film nucleation. We have previously performed simulations to study the impact of molecular hydrocarbon clusters on hydrogen-terminated and bare diamond (111) surfaces [36–41]. Typical results include the displacement of surface hydrogen atoms, the dissociation of cluster molecules into fragments, and the scattering or adhesion of those fragments to the surface in the form of short chains. Film nucleation has been shown to depend on reaction conditions such as molecular reactivity [36], incident velocity [36,37], cluster size [37], and surface reactivity [38,39]. The results showed that the cluster molecules underwent numerous addition reactions when cluster external kinetic energies were within 3 eV/molecule of the binding energy of the individual cluster molecules.

The consecutive impact of two larger (64-molecule) acetylene clusters on hydrogen-terminated diamond (111) surfaces, H:C(111) at incident energies of approximately 20 eV/molecule has also been considered [40]. The simulations predicted that some of the film created from the first cluster collision was sputtered away as the second cluster impacted, while the rest continued to react and form new chemical products. Our more recent work has modeled the growth of polyethylene thin films from the consecutive impact of small (eight-molecule) ethylene clusters on H:C(111) [41]. We impacted a beam of four clusters at incident energies of 50 eV/molecule, which is in the energy range used by Usui et al. [29]. Results included the formation of a crater at the impact site on the surface, partial adhesion of cluster atoms to the surface, and partial sputtering of adhered atoms by impinging and scattering atoms. Crater formation activated some of the surface atoms and permitted better adhesion of the cluster atoms. The resulting film was polymer-like, though the oligomers formed were too short to be considered polymers.

In this paper we now build on our previous results. The system has been expanded so that 20 eight-molecule clusters impact a H:C(111) surface. The effect of incident velocity on crater formation is also investigated as we deposit at incident energies of 25 and 50 eV/molecule. To determine the possible benefits or disadvantages of cluster beam deposition at these incident energies, similar beams of single ethylene molecules are deposited on the same surface. The resulting thin-film fragments are further relaxed through geometry optimization with the quantum semiempirical AM1 method. Finally, the effect of substrate temperature on ethylene cluster impacts on H:C(111) is quantitatively investigated.

2. Computational details

2.1. The REBO potential

The simulation approach is classical molecular dynamics (MD), where Newton's equations of motion are integrated with a Nordsiek predictor corrector [42] using a time step of 0.20 fs. A reactive empirical bond order (REBO) potential for hydrocarbons is used to predict the short-range forces on the atoms in both the clusters and surface [43]. The specific version used is a 'second generation' version of the covalent REBO potential [44–46] that includes both improved analytic functions for the intramolecular interactions and an expanded fitting database. It accurately reflects the energies, bond lengths, and lattice constants for the solid state and gas-phase materials used in this simulation. In addition, a Lennard–Jones (LJ) potential is used to model the carbon–carbon van der Waals bonds in the molecular organic clusters [45]. This LJ potential is only non-zero at distances that are large enough that the REBO potential equals zero.

The second generation of the REBO potential differs from the first generation [43] in that it contains a greatly improved characterization of bond energies, bond lengths and, most especially, force constants for carbon–carbon bonds as compared to the original version of the potential. This has produced an improved fit to the elastic properties of diamond and graphite so that the potential provides better predictions for the energies of several surface reconstruction structures and interstitial defects. The forces associated with rotation about dihedral angles for carbon–carbon double bonds as well as angular interactions associated with

hydrogen centers have also been included for the first time.

The general analytic form for the covalent terms expresses the chemical binding energy E_b as a sum over nearest neighbors in the form

$$E_b = \sum_i \sum_{j(>i)} \left[V^R(r_{ij}) - \bar{b}_{ij} V^A(r_{ij}) \right] \quad (1)$$

where the functions $V^R(r)$ and $V^A(r)$ are two-body interaction terms that represents all interatomic repulsions (core–core, electron–electron) and the attraction from valence electrons, respectively. The variable r is the distance between pairs of nearest-neighbor atoms and b_{ij} is a many-body bond order term between atoms i and j.

The bond order tem consists of parameterized analytic forms and is assumed to depend both on the local coordination and on bond angles, where the latter was necessary to accurately model elastic properties and defect energies. The general form for the bonding energy shown in Eq. (1) is used for the total potential energy. Following the earlier hydrocarbon bonding expression [43], the empirical bond-order function is written as the sum of terms:

$$\bar{b}_{ij} = \frac{1}{2}[b_{ij}^{\sigma-\pi} + b_{ji}^{\sigma-\pi}] + b_{ij}^{\pi} \quad (2)$$

where the values for the functions $b_{ij}^{\sigma-\pi}$ and $b_{jj}^{\sigma-\pi}$ depend on the local coordination and bond angles for atom i and j, respectively, thus insuring that the bond order function is many-body. The function b_{ij}^{π} is expressed as a sum of two terms:

$$b_{ij}^{\pi} = \prod_{ij}^{RC} + b_{ij}^{\mathrm{DH}} \quad (3)$$

where the value of the first term Π_{ij}^{RC} depends on whether a bond between atoms i and j has radical character and is part of a conjugated system. The value of the second term $\mathrm{b}_{ij}^{\mathrm{DH}}$ depends on the dihedral angle for carbon–carbon double bonds. This expression combined with Eq. (1) is used to define the binding energy due to covalent bonding of any collection of hydrogen and carbon atoms. In contrast to a traditional valence-force field method, no predetermined atomic hybridizations are assumed. Rather, the atomic bonding is determined strictly from local bonding neighbors and non-local conjugation. This allows the local bonding environment to determine the effective interatomic interactions so that the influence of atomic rehybridization on the binding energy can be modeled as covalent bonds break and reform within a classical potential.

The specific analytic forms for the pair terms in this version of the REBO potential are as follows:

$$V^R(r) = f_{ij}(r)(1 + Q/r) A e^{-\alpha r} \quad (4)$$

$$V^A(r) = f_{ij}(r) \sum_n b_n e^{-\beta_n r} \quad (5)$$

where the subscripts i and j refer to the sum in Eq. (1), the subscript n refers to the sum in Eq. (5), and r_{ij} is the scalar distance between atoms i and j. The screened Coulomb function used for the repulsive pair interaction in Eq. (4) goes to infinity as interatomic distances approach zero. Furthermore, the attractive term in Eq. (5) has increased flexibility to simultaneously fit the bond properties that could not be fit with the Morse-type terms used in the first generation of the REBO potential [43]. The function $f(r)$ limits the range of the covalent interactions, such that the parameter fitting for carbon assumes a value of one for $f(r)$ for nearest neighbors and zero for all other interatomic distances.

The data base used for fitting the parameters include equilibrium distances, energies, and stretching force constants for single (from diamond), conjugated double (from graphite), full double (from ethylene) and triple (from acetylene) bonds. Further details of the fitting of these functional forms are given in the literature [44–46].

In most cases, this potential has been shown to provide reasonable predictions [45,47–58]. However, as is the case for all empirical potentials, there are cases where the quantitative accuracy is lacking even while the qualitative trends are correct. For example, Hase and co-workers [59] have shown that the REBO potential predicts association potentials for $H + CH_3$ and H + diamond (111) that are significantly smaller than ab-initio values because of the potential's shorter range. Within the REBO potential cutoff, the predicted association potentials are similar to the ab-initio values [59]. This effect is not of significant concern in the present study because of the relatively high incident energies used that bring the clusters or molecules into close contact with each other and the surface (well within the potential cutoff) prior to any reaction.

2.2. Simulation details

The molecular beam consists of 160 single ethylene molecules randomly distributed in a beam that is approximately 22 Å in diameter. The molecules are separated from one another by approximately 6 Å and the beam starts off positioned approximately 4 Å above the surface. Similarly, the cluster beam is created from the repetition of a single cluster on a three-dimensional

grid. The clusters are formed by arranging eight ethylene molecules on a three-dimensional grid and increasing the temperature to 400–500 K while constraining the molecules with three-dimensional periodic boundary conditions [42]. After the cluster has disordered completely, it is quenched to 5 K and replicated to create a beam of 20 clusters, where each cluster is positioned approximately 4 Å above the other. The clusters are randomly oriented relative to each other so that they do not impact the surface with the same orientation or at the same point on the surface. The beam is roughly cylindrical with a diameter of 22 Å and is positioned approximately 4 Å above the surface.

Thus, both the molecular beam and cluster beam systems consist of 960 atoms in the 160 impacting ethylene molecules and a H:C(111) surface with 5824 atoms. The non-rigid surface consists of 26 layers of atoms, with a 33×33 Å surface area exposed to the impacting clusters. The top and bottom layers are composed of hydrogen and the remaining 24 layers are carbon. The lowest 15 layers (one hydrogen and 14 carbon) have Langevin frictional forces [42] applied to them to simulate the heat dissipation in a real diamond surface and to maintain the temperature of the surface at 300 K. Langevin forces are also applied to three to four rows of atoms on the edges of the surface slab. Thus, in total, 4544 of the 5824 surface atoms are Langevin atoms. The remaining surface atoms and all of the cluster atoms are allowed to evolve in time with no additional constraints placed on them. Periodic boundary conditions are also applied within the plane of the surface. Several surface configurations were tested to determine the minimum depth of the surface that would correctly mimic the energy dissipation of a real diamond surface. The 26-layer surface prevented the artificial rebounding of the impact energy from interfering with the surface reaction at the highest incident energies.

The simulations conducted to study the effect of substrate temperature were carried out on a slightly different system. In light of computer memory and run-time limitations, a single cluster consisting of 64 ethylene molecules was impacted on H:C(111). Again, the cluster was formed by equilibrating the molecules at 400–500 K and quenching them to 5 K. This substrate has 3136 atoms and consists of 14 layers of atoms, with a 33×33 Å surface area exposed to the impacting cluster. The lowest two layers (one hydrogen and one carbon) are held rigid, while the next three carbon layers and three to four layers around the sides of the surface are made up of Langevin frictional force atoms (total of 1748). Only low-incident energies were considered to determine the effect of substrate temperature on adhesion, so this configuration is adequate to prevent the rebounding of the incident energy. The cluster is positioned approximately 4 Å above the surface at the start of each trajectory. Each simulation runs for a total of 16 ps, where the time for the film to equilibrate after deposition is approximately four times as long as the deposition period.

3. Results

3.1. Cluster-beam impact results

The initial incident energy considered is 50 eV/molecule, or 400 eV/cluster. As the first few clusters impact the surface, linear chains form that are approximately 6–10 carbon atoms in length. However, almost none of these initial products remain on the surface due to bombardment from the ongoing collisions. Dissociation from the surface occurs either due to increases in the internal energy of these products (evidenced through large atomic vibrations), or through direct collisions of incident clusters with the products. Once the beam impacts are complete, the film structure takes shape from the remaining scattered fragments. A relaxation period of 1.43 ps allows fragments to join and further react with the surface (total simulation time was approx. 3 ps). Most of the film is concentrated near the impact zone with only a few atoms deposited on the edges of the surface. A hemispherical crater that is approximately 16 Å in diameter and 5 Å deep is formed in the surface from the force of the collisions. The final film extends approximately 6 Å above the surface and is composed primarily of atoms that were either formerly part of the diamond lattice or from the latter half of the impact beam.

Fig. 1a depicts a cross-section of the film, and illustrates the depth of the crater formed in the substrate. Approximately 19% of the impinging carbon atoms have filled in the crater (below the top hydrogen layer) in a network formation. Including these atoms, approximately 52% of all the impinging carbon atoms remain adhered to the surface. However, the atoms deposited in the crater are not considered in the analysis of the film structure, though the atoms displaced from the crater that reattach to the surface and extend above it are included. The film consists of carbon that is 33% sp-hybridized, 48% sp^2-hybridized and 14% sp^3-hybridized. The remaining 5% of the carbon atoms in the film have a coordination of 1 because they are either on the end of a chain or are part of a fragment that is in the process of dissociating and re-associating with other atoms in the film.

To determine some of the effects that lead to crater formation, the same simulation is repeated with a cluster beam that has a diameter that is half as large as the diameter of the beam discussed above. A crater is again formed within the impact zone, this time with a diameter of 12 Å and a depth of 8 Å. In this simulation, approximately 65% of the impinging atoms are at-

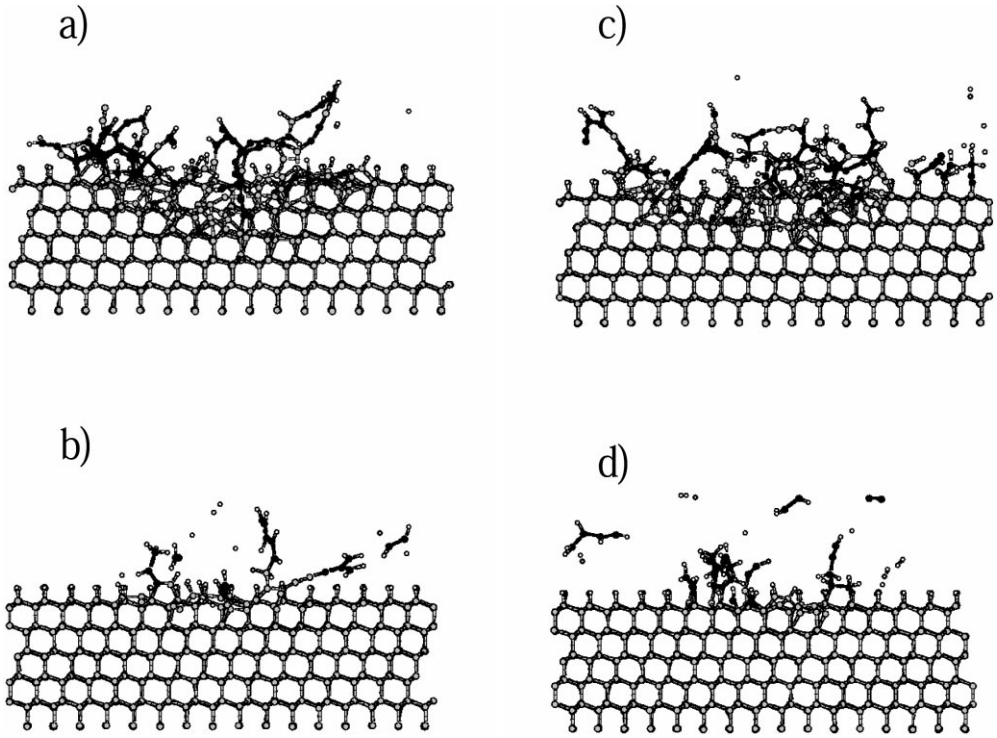

Fig. 1. Snapshots of surface cross sections after deposition on the diamond (111) surface. Only a portion of the surface is shown for clarity. Grey spheres represent diamond lattice atoms, black spheres represent impacting carbon atoms, and white spheres represent hydrogen. (a) Cluster beam impacted at 50 eV/molecule at time = 2.70 ps. (b) Cluster beam impacted at 25 eV/molecule at time = 4.10 ps. (c) Molecular beam impacted at 50 eV/molecule at time = 2.9 ps. (d) Molecular beam impacted at 25 eV/molecule at time = 5.70 ps.

tached to or embedded in the surface after impact. The film structure is very similar to that formed with the wider beam.

A simulation with the 22 Å-beam diameter is also performed at an incident kinetic energy of 25 eV/molecule, or 200 eV/cluster. More of the chains that are formed as a result of these collisions remain attached to the surface even as the beam continues to bombard it. Throughout the simulation, only five to six surface carbon atoms are detached from the diamond lattice and no crater is formed. Most chains are three to four carbon atoms in length and are distributed around the impact area, again concentrated near the center. Fig. 1b shows a cross-section of this film. Roughly 13% of the impacting carbon cluster atoms adhere to the surface as a film that extends approximately 5 Å above the surface. The final film is made up of an even distribution of atoms from all positions in the cluster beam and consists of carbon that is 13% sp-hybridized, 47% sp^2-hybridized, and 40% sp^3-hybridized.

3.2. Molecular-beam impact results

Under conditions that are very similar to those of the first cluster beam considered above, a molecular beam is impacted at 50 eV/molecule. A few small chains five to six atoms in length survive the impact stage. Once relaxation is complete, the film consists of tethered chains eight to nine carbon atoms in length that are distributed around the rim of the impact zone. In addition, a few fragments have extended to the edge of the surface. Compared to the cluster beam, 32% fewer surface atoms have been sputtered away, resulting in a crater with a diameter of 15 Å and a depth of 4 Å. Fig. 1c illustrates a cross-section of the film and crater. The film consists of an even distribution of atoms from all parts of the beam and the surface. Approximately 60% of the impinging cluster atoms adhere to or embed in the surface. The final film consists of 31% sp, 55% sp^2 and 10% sp^3-bonded carbon atoms arranged in short chains that extend approximately 5 Å above the surface. The remaining 4% of the carbon atoms in the film have a coordination that is less than 2 because they are either at the end of a chain or are part of a fragment that is in the process of dissociating and re-associating with the film.

Next the same collision is repeated at incident energies of 25 eV/molecule. Once relaxation is complete, the film consists of single three to four atom chains that extend upward about 3 Å located at evenly spaced intervals across the surface as shown in Fig. 1d. Only approximately 18% of the impacting carbon atoms adhere to the surface. The film consists of carbon with

15% sp-, 54% sp^2-, and 31% sp^3-type bonding. The film is made up of an even distribution of atoms from all positions in the beam and no surface atoms are permanently moved from their original position in the lattice.

3.3. Surface temperature effects on adhesion

A series of simulations were performed to assess the effect of substrate temperature on the adhesion of the products of ethylene clusters deposited on the H:C(111) surface as a function of surface temperature. Temperatures studied are 5 K, 300 K, 500 K, 900 K and 1200 K. In each case a 64-molecule cluster is deposited with an incident energy of 23 eV/molecule at different locations on the surface. No crater formation was observed in any of these trajectories. For each surface temperature considered, this deposition was performed eight times from slightly different starting configurations. The eight results for each temperature are averaged and plotted in Fig. 2. A slight increase in film formation is observed as the substrate temperature increases, though the difference is only 3% over the 1195° temperature range considered, which is within the errorbars for these results.

More than half of the cluster's external energy is transferred to the surface as internal kinetic energy upon impact. This results in localized heating of the impact zone on the surface to several thousand degrees before the excess energy is dissipated by the Langevin frictional forces. This is the main reason why the starting substrate temperature has little effect on the chemical reactions at the surface. However, it should be noted that substrate temperature could have an effect on the relaxation of thin films over long times (several seconds, minutes, or hours) that can not be accessed by conventional molecular dynamics simulations such as those used here.

3.4. Continued relaxation of thin-film fragments with force-field model

In order to check the stability of the thin-film structures that result from the cluster-beam and molecular-beam deposition, geometry relaxation through energy minimization has been performed for two representative fragments each from the high and low velocity bombardment. The fragments chosen are representative of the results of both cluster-beam and molecular-beam deposition. The goal is to identify the fragment configurations that correspond to energy minima without regard to time. To simulate minimum energy configurations we used a cluster model and the quantum, semiempirical AM1 method [60] that has been shown to have good accuracy when applied to non transition-metal systems.

The AM1 method was selected because it is different

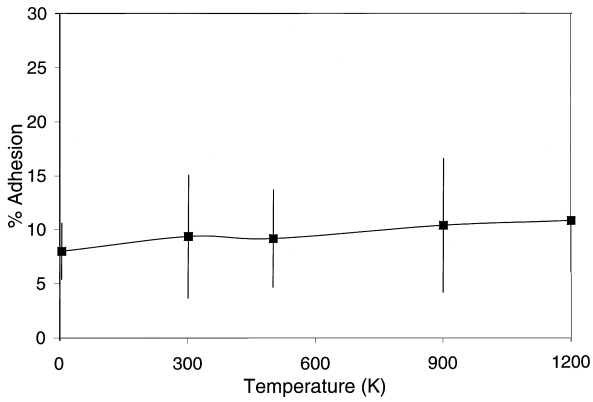

Fig. 2. Percent adhesion of impacting carbon atoms as a function of substrate temperature. The data is averaged over eight trajectories at each temperature.

from the REBO method and thus provides a check of the structural stability of the thin-film fragments and at the same time requires substantially less rigorous use of computational resources than comparable ab-initio or density functional theory approaches. In addition, AM1 provides information about properties connected with electronic structure such as charge population, bond orders, and dipole moments. It can therefore be applied regardless of the presence of charges in the structure, unlike the fully classical REBO potential. The AM1 method has become even more widely used since it has been incorporated in such well-known commercial software packages as GAUSSIAN and HYPERCHEM.

It has been shown that the reliability of the AM1 method very often depends on the size and the shape of clusters [61,62]. As already noted above, the high-velocity scattering resulted in dramatic surface damages (craters) that are difficult to model in slab structures containing only a few atoms. Therefore the final high-velocity structures include portions of the original damaged surface. The slab was cut out of the simulation surface such that the linear size of the surface is at a minimum no less than the linear size of the adsorbed species positioned in the center (see Fig. 3). The surface was saturated with hydrogen atoms to avoid edge effects. The resulting structures have a maximum of 207 atoms.

Despite this relatively small size, it is still too large to allow for the timely use of ab-initio or density functional theory methods to optimize the structures. At the same time, since the selected thin-film structures are just representative of many other cases it is not our intention to determine their exact geometry and energies. Rather, the goal is to determine the final relaxed structure of the thin-film fragments and hypothesize as to some of the additional reactions that could occur over long times. To further decrease the amount of computational effort and maintain the shape of the

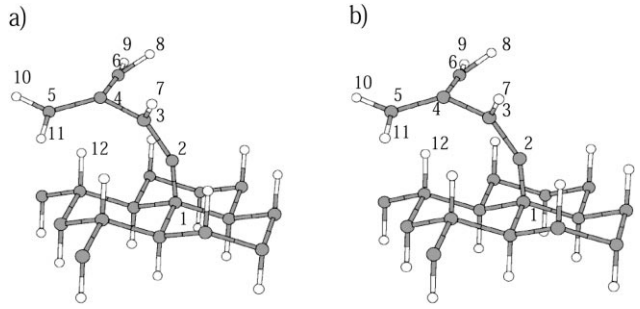

Fig. 3. Representative thin-film fragment from the 25 eV/molecule bombardment simulations termed cluster 1 (a) before and (b) after AM1 geometry optimization.

surface cluster, the surface atoms are held rigid and only the atoms in the adsorbed thin-film fragment and a few surface atoms surrounding the adsorption site are allowed to move to minimize their energy. All the structures considered have been successfully optimized and have reached at least a local minimum.

For the fragments from the low impact velocities of 25 eV/molecule it is seen that the geometry corresponding to the calculated minimum energy is almost the same as the one obtained by the REBO potential, as shown quantitatively in Table 1 and qualitatively in Figs. 3 and 4. The results of Mulliken electron charge population analysis for the minimized energy structures are given in Table 2. While Mulliken population analysis provides data that can not be directly measured experimentally, it does provide detailed information about bond-orders and charges on atoms that can be useful in determining reactivity. For these fragments, the Mulliken population analysis shows that the larger charges are localized at the atoms with higher reactive probability to capture a hydride radical. It is well known that methyl carbon (such as carbon atoms 5,6 in cluster 1 in Fig. 3, and carbon atom 4 in cluster 2 in Fig. 4) form bonds more easily to single H atoms than comparable methylene carbon atoms. In other words, a CH_2–R radical can more easily capture a H radical to from a methyl carbon than R–CH–R can capture a H radical to form a methylene carbon. The most probable and well-studied reactions with the lowest energy barriers could involve (1) hydride migration (from carbon number 3 to carbon number 2 in cluster 1 and from carbon number 3 to carbon number 4 in cluster 2) [63]; (2) hydride exchange and/or hydride donation (between carbon number 5 and a surface carbon atom in cluster 1 and carbon number 4 and a surface carbon in cluster 2 [64]; and (3) activation of one of the carbon–carbon bonds followed by cleavage-cracking of the bond [65].

At the higher velocity bombardment of 50 eV/molecule, the change in geometry of the adsorbed species is larger than at low impact velocity though this change is still not significant. Figs. 5 and 6 and Table 3 contain details about the structure of a typical fragment of adsorbed thin-film before and after geometry optimization. The geometry changes enough to allow one carbon–carbon bond to break and for the formation of four new bonds to the surface for cluster 3 (carbon atoms 1,2,3; 6,7,8; 14,15,16; 17,18,19). In addition, two new bonds are formed in cluster 4 (carbon atoms 18,21). These new bonds stabilize and strengthen the base of the thin-film structure changing the orbital hybridization of a few atoms from sp to sp^2 and eliminating some dangling bonds. At the same time the adsorbed species itself straightens in the vertical direction, as seen in both Figs. 5 and 6. This compresses the carbon–carbon bond lengths due to sp hybridization and correspondent 'double' and 'triple' bonding between carbon atoms similar to what is found in ethylene and acetylene molecules (bonds 3–4, 4–5 and 10–11, 12–13, respectively, in cluster 3 and 13–14, 14–15 in cluster 4).

The Mulliken charge population for these clusters is given in Table 4. Again the Mulliken atomic charges give some evidence about atoms which could bond to

Table 1
Bond lengths and bond angles in the low impact energy thin-film structures that underwent geometry optimization using AM1[a]

Atom number	Cluster 1		Cluster 2	
	MD geometry	AM1 geometry	MD geometry	AM1 geometry
1–2	1.16 Å	1.40 Å	1.40 Å	1.46 Å
2–3	1.33 Å	1.23 Å	1.58 Å	1.54 Å
3–4	1.44 Å	1.52 Å	1.40 Å	1.43 Å
4–5	1.38 Å	1.39 Å		
4–6	1.42 Å	1.37 Å		
11–12	1.46 Å	1.46 Å	1.82 Å	1.79 Å
1–2–3	151.4°	143.7°	115.8°	116.3°
2–3–4	129.7°	134.3°	114.0°	113.5°
3–4–5	116.7°	117.5°		
5–4–6	128.9°	131.9°		

[a]Clusters 1 and 2 are shown in Figs. 3 and 4, respectively.

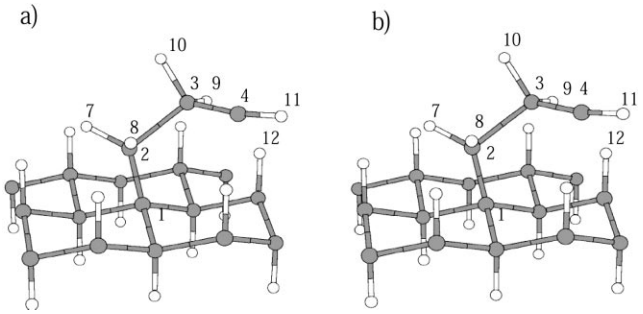

Fig. 4. Representative thin-film fragment from the 25 eV/molecule bombardment simulations termed cluster 2 (a) before and (b) after AM1 geometry optimization.

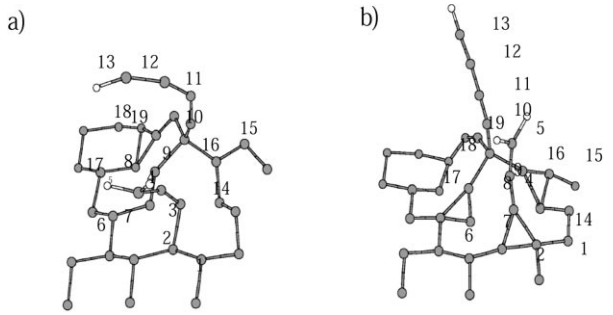

Fig. 5. Representative thin-film fragment from the 50 eV/molecule bombardment simulations termed cluster 3 (a) before and (b) after AM1 geometry optimization.

other chains or atoms. The methyl carbon atoms on the edges (carbon atoms 5 and 13 except for carbon number 9 in cluster 3, and carbon atom 15 in cluster 4) have higher electron populations than the other carbon atoms in the fragment. In addition, very small charges on the other atoms could provide evidence about the relative stabilities of the systems (similar to the stabilities of ethylene and acetylene).

4. Discussion and conclusions

This paper has examined the growth of polyethylene thin films via molecular-beam and cluster-beam deposition on hydrogen-terminated diamond (111) using molecular dynamics simulations. The results demonstrate differences in rates of nucleation, damage to the substrate, and the character of the hydrocarbon films formed that depend on the type of beam used and/or the incident energies. The simulations predict that at the hyperthermal incident energies used in this study, substrate temperature does not have a significant effect on the results.

At the highest incident energies considered of 50 eV/molecule, the molecular beam yields a film that consists primarily of short linear and branched (sp^2-hybridized carbon) chains attached to the substrate, as summarized in Fig. 7. Crater formation in the surface is 30% less than the crater that forms during cluster-beam deposition and the film is evenly distributed around the impact zone. At the same impact velocity, the cluster beam forms a deeper crater and a less even film that nevertheless has a similar structure (see Fig. 7). Because the clusters sputter off more of the film during growth, less surface damage and a more even film is predicted to grow during molecular-beam deposition relative to cluster-beam deposition. However, the difference in the amount of thin-film nucleation that is predicted to occur during the cluster-beam deposition relative to the molecular-beam deposition is insignificant at both the incident energies considered.

Beam diameter is also predicted to have a small effect on crater depth, with slightly more carbon atoms deposited at the bottom of the crater than on the surface when the beam diameter is halved. In a previous study [40], the effect of time between the impact of larger molecular clusters was investigated and found to have negligible effect on the structure of the film. However, shorter times between impacts resulted in larger surface damage. It is expected that this is true in this study as well although the effect of deposition rate was not explicitly addressed in this work.

At lower impact energies of 25 eV/molecule, the

Table 2
Mulliken population analysis data for the low impact energy thin-film structures that underwent geometry optimization using AM1[a]

Atom number	Mulliken net charges	
	Cluster 1	Cluster 2
C1	−0.03	−0.03
C2	−0.15	−0.27
C3	−0.20	−0.16
C4	−0.07	−0.50
C5	−0.34	
C6	−0.41	
H7	0.22	0.15
H8	0.25	0.15
H9	0.09	0.17
H10	0.18	0.11
H11	0.22	0.30
H12	0.28	0.14

[a] Clusters 1 and 2 are shown in Figs. 3 and 4, respectively.

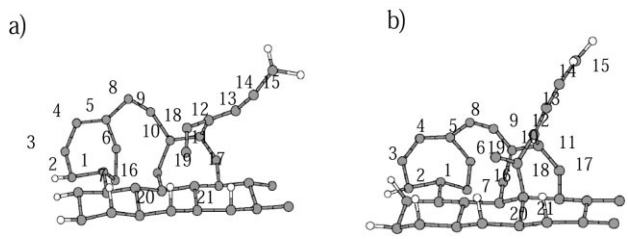

Fig. 6. Representative thin-film fragment from the 50 eV/molecule bombardment simulations termed cluster 4 (a) before and (b) after AM1 geometry optimization.

Table 3
Bond lengths and bond angles in the low impact energy thin-film structures that underwent geometry optimization using AM1[a]

	Cluster 3		Cluster 4	
	MD geometry	AM1 geometry	MD geometry	AM1 geometry
1–2	1.58 Å	1.52 Å	1.52 Å	1.61 Å
2–3	1.67 Å	1.52 Å	1.44 Å	1.42 Å
3–1	2.04 Å	1.46 Å		
3–4	1.39 Å	1.28 Å	1.34 Å	1.24 Å
4–5	1.35 Å	1.30 Å	1.43 Å	1.36 Å
5–6			1.49 Å	1.56 Å
6–7	1.51 Å	1.49 Å	1.65 Å	1.63 Å
7–8	1.35 Å	1.32 Å		
6–8	2.25 Å	1.54 Å	2.53 Å	2.33 Å
8–9	1.58 Å	1.52 Å	1.36 Å	1.22 Å
9–10	1.44 Å	1.43 Å	1.52 Å	1.38 Å
10–11	1.35 Å	1.23 Å	1.53 Å	1.45 Å
11–12	1.25 Å	1.32 Å	1.53 Å	1.47 Å
12–13	1.46 Å	1.23 Å	1.41 Å	1.30 Å
13–14			1.34 Å	1.26 Å
14–15			1.32 Å	1.30 Å
10–16			1.53 Å	1.40 Å
11–17			1.38 Å	1.35 Å
12–18			1.40 Å	1.49 Å
18–19			1.32 Å	1.33 Å
18–21			2.57 Å	1.52 Å
1–2–3	77.7°	57.3°	106.3°	107.5°
2–3–4	120.4°	156.4°	130.7°	123.4°
3–4–5	156.8°	167.6°	120.4°	127.0°
4–5–6			109.0°	115.8°
5–6–7			116.9°	98.0°
5–8–9			117.2°	138.2°
8–9–10	116.6°	114.2°	148.4°	149.6°
9–10–11	158.4°	167.8°	120.1°	130.5°
10–11–12	131.3°	178.7°	131.3°	123.1°
11–12–13	158.0°	176.5°	138.6°	131.1°
12–13–14			157.4°	174.0°
13–14–15			153.5°	174.6°

[a]Clusters 3 and 4 are shown in Figs. 5 and 6, respectively.

thin-film adhesion is approximately one-third less than at the higher velocity. There is no crater formation at this incident energy for either of the beams considered. Hybridization within the film is similar in the films formed when the two types of beams are impacted at the same energy. However, the lower energy beams have approximately 20% more sp^3 character than the higher energy beams, as shown in Fig. 7.

These results show that film growth is clearly more rapid at higher impact energies, though at these conditions both cluster and molecular beam deposition cause damage to the surface. At lower incident energies, where crater-formation does not occur, there is less adhesion of the incident molecules and the products of their reactions. In addition, the lower impact energy collisions form films with more diamond-like character while the higher impact energy collisions yield films with more polymer-like character, as evidenced by a predominance of linear and branched chains.

Long-term relaxation could affect the film structure and therefore geometry optimization using energy minimization with the quantum semiempirical AM1 is performed. The results show some changes in the structures and identify the most reactive atoms in the thin-film fragments. This provides information about the possible reactions the fragments could undergo in air or on exposure to additional reactant beams. The conclusion of these minimization studies is that although the thin-film fragment geometries change only slightly during geometry optimization, it is predicted that the structure of the fragments will change significantly on exposure to air.

Table 4
Mulliken population analysis data for the high impact energy thin-film structures that underwent geometry optimization using AM1[a]

Atom number	Mulliken net charges	
	Cluster 3	Cluster 4
C1	−0.07	0.01
C2	−0.03	−0.05
C3	−0.01	−0.16
C4	−0.10	−0.12
C5	−0.25	0.17
C6	0.01	0.06
C7	−0.17	−0.02
C8	−0.04	−0.13
C9	0.39	−0.03
C10	−0.08	0.10
C11	−0.04	−0.04
C12	−0.06	0.09
C13	−0.24	−0.09
C14		−0.08
C15		−0.25

[a]Clusters 3 and 4 are shown in Figs. 5 and 6, respectively.

In conclusion, cluster-beam deposition is not predicted to provide improved thin-film growth relative to molecular-beam deposition and, in fact, causes increased surface damage at higher incident energies. Thus, the incentive to use clusters for thin-film growth mentioned by some researchers [9,16,17,29] is not born out in these simulations.

Acknowledgements

The authors thank Donald Brenner and W. Leigh Young for many helpful discussions. This work was supported by the National Science Foundation (CHE-9708049) and the donors of the Petroleum Research Fund (administered by the American Chemical Society).

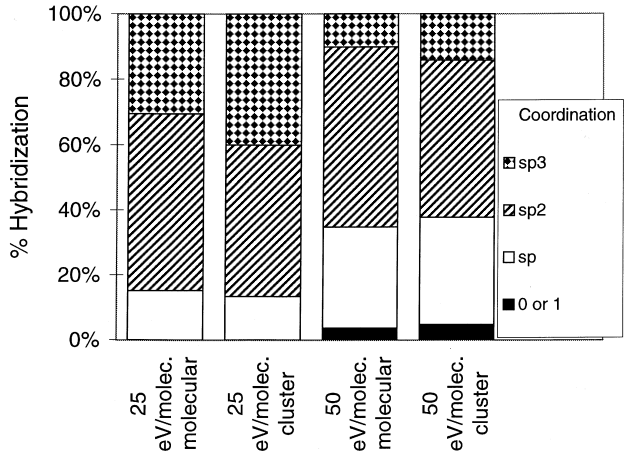

Fig. 7. Summary of the bonding character (hybridization) of the carbon atoms in the hydrocarbon films formed by molecular-beam and cluster-beam deposition.

References

[1] A. Zangwell, Physics at Surfaces, Cambridge University Press, New York, 1990.
[2] W.L. Brown, M. Sosnowski, Nucl. Inst. Meth. B102 (1995) 305.
[3] W.L. Brown, R.R. Freeman, K. Raghavachari, M. Schluter, Science 235 (1987) 860.
[4] A.W. Castleman Jr., K.H. Brown, Jr., J. Phys. Chem. 100 (1996) 12911.
[5] C.L. Kelchner, A.E. DePristo, NanoStructured Mater. 8 (1997) 253.
[6] J.A. Niesse, J.N. Beauregard, H.R. Mayne, J. Phys. Chem. 98 (1994) 8600.
[7] G.-Q. Xu, R.J. Holland, S.L. Bernasek, J.C. Tully, J. Chem. Phys. 90 (1989) 3831.
[8] T. Raz, I. Schek, M. Ben-Nun, U. Even, J. Jortner, R.D. Levine, J. Chem. Phys. 101 (1994) 8606.
[9] C.L. Cleveland, U. Landman, Science 257 (1992) 355.
[10] Z. Insepov, I. Yamada, Nucl. Inst. Meth. B 121 (1997) 44.
[11] T. Aoki, J. Matsuo, Z. Insepov, I. Yamada, Nucl. Inst. Meth. B 121 (1997) 49.
[12] H.J. Kang, M.W. Lee, J.H. Kim, C.N. Whang, Nucl. Inst. Meth. B 121 (1997) 53.
[13] F.J. Palacios, M.P. Iniguez, M.J. Lopez, J.A. Alonso, Phys. Rev. B 60 (1999) 2908.
[14] C.-C. Fu, M. Weissmann, Phys. Rev. B 60 (1999) 2762.
[15] D. Donadio, L. Colombo, P. Milani, G. Benedek, Phys. Rev. Lett. 83 (1999) 776.
[16] H. Haberland, M. Karrais, M. Mall, Y. Thurner, J. Vac. Sci. Technol. A 10 (1992) 3266.
[17] H. Hsieh, R.S. Averback, H. Sellers, C.P. Flynn, Phys. Rev. B 45 (1992) 4417.
[18] G. Vandoni, C. Felix, C. Massobrio, Phys. Rev. B 54 (1996) 1553.
[19] M.H. Shapiro, G.A. Tosheff, T.A. Tombrello, Nucl. Inst. Meth. B88 (1994) 81.
[20] H. Haberland, Z. Insepov, M. Moseler, Phys. Rev. B 51 (1995) 11061.
[21] H. Haberland, M. Mall, M. Moseler, Y. Qiang, T. Reiners, Y. Thurner, J. Vac. Sci. Technol. A 12 (1994) 2925.
[22] N.C. Blaise, J.R. Stine, J. Chem. Phys. 93 (1990) 7914.
[23] T. Raz, I. Schek, M. Nen-Nun, U. Even, J. Jortner, R.D. Levine, J. Chem. Phys. 101 (1994) 8606.
[24] F. Huisken, B. Kohn, V. Paillard, Appl. Phys. Lett. 74 (1999) 3776.
[25] K. Kakishita, S. Kondo, T. Suda, Nucl. Inst. Meth. B 121 (1997) 175.
[26] H.J. Gao, A.Q. Xue, K.Z. Wang, Q.D. Wu, S. Pang, J. Appl. Phys. 68 (1996) 2192.
[27] H.J. Gao, Z.Q. Xue, K.Z. Wang, Q.D. Wu, S. Pang, Appl. Phys. Lett. 68 (1996) 2192.
[28] V. Paillard, P. Milinon, V. Dupuis, J.P. Perez, A. Perez, B. Champagnon, Phys. Rev. Lett. 71 (1993) 4170.
[29] H. Usui, I. Yamada, T. Takagi, J. Vac. Sci. Technol. A 4 (1986) 52.
[30] A. Fejfar, H. Biederman, Int. J. Elect. 73 (1992) 1051.
[31] N. Yamaguchi, Y. Sasajima, K. Terashima, T. Yoshida, Thin Solid Films 345 (1999) 34.
[32] B.K. Tay, X. Shi, E.J. Liu, H.S. Tan, L.K. Cheah, Thin Solid Films 346 (1999) 155.
[33] M. Chhowalla, J. Robertson, S. Silva, C. Davis, G. Amaratunga, W. Milne, J. Appl. Phys. 81 (1997) 139.
[34] S. Sattel, J. Robertson, H. Ehrhardt, J. Appl. Phys. 82 (1997) 4566.
[35] N.H. Cho, D. Veirs, J. Ager, M. Rubin, C. Hopper, J. Appl. Phys. 71 (1992) 2244.
[36] L. Qi, S.B. Sinnott, J. Phys. Chem. B 101 (1997) 6883.

[37] L. Qi, S.B. Sinnott, Nucl. Inst. Meth. B 140 (1998) 39.
[38] L. Qi, S.B. Sinnott, J. Vac. Sci. Technol. A 16 (1998) 1293.
[39] L. Qi, W.L. Young, S.B. Sinnott, Surf. Sci. 426 (1999) 83.
[40] L. Qi, S.B. Sinnott, Surf. Sci. 398 (1998) 195.
[41] T.A. Plaisted, J.D. Zahrt, W.L. Young, L. Qi, S.B. Sinnott, in: J.L. Duggan, I.L. Morgan (Eds.), Proceedings of the Fifteenth International Conference, Denton, Texas, November, 1998, AIP Conference Proceedings 475 (1999) 387.
[42] M.P. Allen, D.J. Tildesley, Computer Simulation of Liquids, Oxford University Press, New York, 1987.
[43] D.W. Brenner, Phys. Rev. B 42 (1990) 9458.
[44] D.W. Brenner, J.A. Harrison, O.A. Shenderova, S.B. Sinnott, J. Phys. C: Condensed Matter in preparation.
[45] S.B. Sinnott, L. Qi, O.A. Shenderova, D.W. Brenner, Advances in classical trajectory methods, in: W. Hase (Ed.), Molecular Dynamics of Clusters, Surfaces, Liquids, and Interfaces, 4, JAI Press, Inc, Stamford, CT, 1999, p. 1.
[46] D.W. Brenner, Phys. Stat. Solidi B 217 (2000) 23.
[47] A.B. Tutein, S.J. Stuart, J.A. Harrison, J. Phys. Chem. B 103 (1999) 11357.
[48] K.S.S. Liu, C.W. Yong, B.J. Garrison, J.C. Vickerman, J. Phys. Chem. B 103 (1999) 3195.
[49] R. Chatterjee, Z. Postawa, N. Winograd, B.J. Garrison, J. Phys. Chem. B 103 (1999) 151.
[50] M.B.J. Wijesundara, L. Hanley, B. Ni, S.B. Sinnott, Proc. Natl. Acad. Sci. USA 97 (2000) 23.
[51] J.A. Harrison, S.J. Stuart, D.H. Robertson, C.T. White, J. Phys. Chem B 101 (1997) 9682.
[52] A. Garg, J. Han, S.B. Sinnott, Phys. Rev. Lett. 81 (1998) 2260.
[53] A. Garg, S.B. Sinnott, Chem. Phys. Lett. 295 (1998) 273.
[54] A. Garg, S.B. Sinnott, Phys. Rev. B 60 (1999) 13786.
[55] D. Srivastava, D.W. Brenner, J.D. Schall, K.D. Ausman, M.F. Yu, R.S. Ruoff, J. Phys. Chem. B 103 (1999) 4330.
[56] O.A. Shenderova, D.W. Brenner, A. Nazarov, A. Romanov, L. Yang, Phys. Rev. B. 57 (1998) R3181.
[57] O.A. Shenderova, D.W. Brenner, L.H. Yang, Phys. Rev. B 60 (1999) 7043.
[58] O.A. Shenderova, D.W. Brenner, A. Omeltchenko, X. Su, L.H. Yang, Phys. Rev. B61 (2000) 3877.
[59] P. DeSainte Claire, K. Son, W.L. Hase, D.W. Brenner, J. Am. Chem. Soc. 100 (1996) 1761.
[60] M.J.S. Dewar, E.G. Zoebisch, E.F. Healy, J.J.P. Stewart, J. Am. Chem. Soc. 107 (1985) 3902.
[61] P.E.M. Siegbahn, U. Wahlgren, X. Shustorovich, Metal-Surface Reaction Energetics: Theory and Applications to Heterogeneous Catalysis Chemisorption and Surface Diffusion, VCH, New-York, 1991.
[62] P.E.M. Siegbahn, U. Wahlgren, Int. J. Quant. Chem. 42 (1992) 1149.
[63] G.K. Surya Prakash, P.R. Schleyer (Eds.), Stable Carbocation Chemistry, Wiley, New York, 1997.
[64] G.J. Kramer, R.A. van Santen, J. Am. Chem. Soc. 117 (1995) 1766.
[65] J.A. Lercher, R.A. van Santen, H. Vinek, Catal. Lett. 27 (1994) 91.